Modelling of Seismoelectric Effects

B. Kröger[*,1], U. Yaramanci[2] and A. Kemna[1].
[1] University of Bonn, Department of Geodynamics and Geophysics
[2] GGA Hannover, Leibniz Institute of Applied Geosciences
*Corresponding author: Nußallee 8, D-53115 Bonn, kroeger@geo.uni-bonn.de

Abstract: We present the results of full-waveform time-dependent finite-element modelling of coupled seismoelectromagnetic wave propagation in fluid-saturated porous media. To describe the seismoelectric response of the system a new set of equations is developed which couple the poroelasticity theory and Maxwell's equations via flux/force transport equations in a thermodynamical sense. The coupling mechanism is of electrokinetic nature involving relative displacement of ions at the matrix-fluid interface in the pore space. Modelling is performed with COMSOL Multiphysics on the basis of a two-dimensional implementation of the coupled equations with a view to an improved understanding of the interactions of the main effects characterizing the coupled seismic and electromagnetic responses. The numerical simulations indicate the potential of exploiting seismoelectromagnetic wave propagation and conversion for the characterization of the subsurface and its fluid content.

Keywords: Geophysics, porous media, seismoelectric, wave propagation.

1. Introduction

As the generation of seismoelectric signals is connected with properties such as hydraulic permeability, porosity and fluid salinity it is possible that the seismoelectric method could be used in hydrogeophysical applications for determining these parameters. The relationship between rock properties directly related to fluid flow on the one hand and electric fields caused by electrokinetic effects on the other hand seems to offer a new approach for measurements especially of the hydraulic permeability.

The theoretical basis of the seismoelectric method was elaborated by Pride in 1994. He derived a set of coupled equations that describe the conversion of energy between the seismic and electromagnetic wave fields. Over the years improved computing capabilities have provided significant progress in modelling (e.g. Haartsen and Pride 1997, Garambois and Dietrich 2002, Haines and Pride 2006). Corresponding results permit valuable insight in the types of contrasts that may be imaged with the seismoelectric method. But many fundamental questions concerning the origin and structure of seismoelectric signals are still unsolved. So a numerical modelling approach remains necessary to understand the interaction of processes which are associated with the seismoelectric effects.

2. Physical approach

2.1 Governing equations

In this paper we use a finite-element modelling algorithm to simulate seismoelectric phenomena in earth models for the main poroelastic wave modes (fast compressional waves and vertical polarized shear waves). The macroscopic governing seismo-electric field equations describe (1) the mechanical wave behaviour, captured in the equations according to poroelasticity theory, and (2) the electromagnetic wave behaviour, captured in Maxwell's equations. The coupling between both physical responses is represented in form of (3) transport equations derived from the thermodynamics of irreversible processes (TIP).

The dynamic responses of fluid-saturated porous continua subject to transient excitations such as seismic waves are usually modelled with Biot`s theory (Biot 1956a). The vector of the solid displacement **u**, the vector of the seepage velocity **w** and the pore pressure p are used to derive these equations. Both from a physical and from a numerical point of view a reduction of variables is desirable. However, in a time-domain representation only a formulation with solid and fluid displacements is possible. Under the assumption of a negligible fluid acceleration relative to the solid, a solid displacement/pore pressure formulation can be obtained. This was shown e.g. by Zienkiewicz et al. 1999. For problems in which high-frequency components are absent, they introduced a simple and efficient formulation based on the displacement of the

solid phase **u** and the pore pressure p as the essential variables and called this the "u-p formulation". Following this assumption, we here introduce a simplified poroelastic model for the seismoelectric effects directly in the time domain. Using a low-frequency approximation, the saturated rock/soil system is modelled as a two-phase material based on the linear poroelasticity theory for porous media (Wang 2000). Introducing the stress-strain relationship plus an incremental change caused by variation of the fluid pressure leads to the constitutive equation for poroelasticity. The equilibrium conditions for volume elements combined with Hooke`s extended law for poroelastic bodies can then be recast as follows:

$$G\nabla^2\mathbf{u} + G/(1-2\nu)\,\nabla(\nabla\cdot\mathbf{u}) = \alpha\nabla p + \rho\,\partial^2\mathbf{u}/\partial t^2 + \rho_f\,\partial^2\mathbf{w}/\partial t^2 \qquad (1)$$

where G is the shear modulus of the solid frame, α the effective stress coefficient (Biot-Willis coefficient), p the excess pore pressure, ν the Poisson number, **u** the total displacement, **w** the relative displacement between fluid and matrix, ρ the bulk density, and ρ_f the fluid density.

For the description of the electromagnetic response of the system Maxwell`s equations are used. In the case of a time-dependent electric field Faraday's law states:

$$\boldsymbol{\nabla}\times\mathbf{E} = \mu\,\partial\mathbf{H}/\partial t, \qquad (2)$$

where **E** is the electric field strength, **H** is the magnetic field strength, and μ the magnetic permeability.

The magnetic field caused by an electrokinetic system can be described by Ampere`s law:

$$\boldsymbol{\nabla}\times\mathbf{H} = \mathbf{j} + \dot{\mathbf{D}} = \sigma\mathbf{E} + L\nabla p + \partial\mathbf{D}/\partial t, \qquad (3)$$

where **D** is the electric displacement, **j** the total current density, and σ the electrical conductivity. The total current density in equation (3) is composed of a conduction current density $\sigma\mathbf{E}$ and a current density $L\nabla p$ caused by charges being dragged by the flowing fluid; the corresponding electric potential is well known as the streaming potential (e.g. Wurmstich and Morgan 1994; Pride 1994). The dielectric displacement current $\partial\mathbf{D}/\partial t$ can be neglected relative to the conduction current density because $\omega\varepsilon/\sigma < 10^{-4}$ for seismic frequencies and materials of interest (Haines and Pride, 2006).

For TIP, the interaction of coupled and direct fluxes leads to so-called electrokinetic phenomena (e.g. De Groot 1960; Groot and Mazur, 1984). The thermodynamic fluxes associated with electrokinetic phenomena (fluid velocity and electrical current density) can be derived in thermodynamic non-equilibrium as a linear combination of thermodynamic forces (hydraulic potential gradient and electrical potential gradient). The laws controlling linear transport in porous media in the presence of electrokinetic coupling are:

$$\mathbf{q} = k/\eta\left(-\nabla p + \rho_f\,\partial^2\mathbf{u}/\partial t^2\right) + L\mathbf{E}\,, \qquad (4)$$

$$\nabla\cdot\mathbf{j} = \nabla\cdot\left[\,L\left(-\nabla p + \rho_f\,\partial^2\mathbf{u}/\partial t^2\right) + \sigma\mathbf{E}\,\right]. \qquad (5)$$

The first term on the right-hand side of equation (4) describes Darcy's law for the hydraulic flow of a fluid with the specific flux **q**, the dynamic viscosity η in a porous rock matrix of hydraulic conductivity k driven by a pressure gradient. This dynamic flux must be extended with respect to pressure differences in the fluid caused by the seismic disturbances (Biot 1956a). The second term on the right-hand side of equation (5) represents Ohm's law and describes the electrical current caused by an electric potential gradient (voltage) in a conductive medium. The remaining terms, which couple the two phenomena, represent the electroosmotic drag exerted on the hydraulic flow caused by the electric voltage and the electrokinetic current density (associated with streaming potential), which is also extended because of the pressure differences in the fluid (Wurmstich and Morgan, 1994). Equation (5) is valid under the assumption of absence of external sources in the system, i.e. $\nabla\cdot\mathbf{j} = 0$. The electrical conductivity is given by $\sigma = \sigma_f/F_0$, where σ_f is the fluid conductivity and F_0 is the formation factor.

The coupling coefficient L ("Onsager coefficient") is dependent on the dielectric permittivity ε_0 of the fluid, the zeta potential ζ associated with the mineral-fluid interface, the formation factor F_0 and the viscosity η:

$$L = -\epsilon_0\epsilon_r\zeta/(F_0\,\eta)\,. \qquad (6)$$

The zeta potential ζ describes the strength of the electric double layer, so the electrokinetic coupling coefficient L depends explicitly on the electric double layer properties (Pride 19994).

Finally, after some algebraic manipulations (Kröger 2007), the reduced set of equations which couple the seismic and electromagnetic responses of the system can be summarized as follows:

$$G\nabla^2\mathbf{u} + G/(1-2\nu)\,\nabla(\nabla\cdot\mathbf{u})$$

$$= \alpha\nabla p + \rho\,\partial^2\mathbf{u}/\partial t^2 \qquad (7)$$

$$\nabla\cdot\left[\, k/\eta\left(-\nabla p + \rho_f\,\partial^2\mathbf{u}/\partial t^2\right) + L\mathbf{E}\right]$$

$$= -\alpha\,\partial(\nabla\cdot\mathbf{u})/\partial t - S_\alpha\,\partial p/\partial t, \qquad (8)$$

$$\nabla\cdot\left[\, L\left(-\nabla p + \rho_f\,\partial^2\mathbf{u}/\partial t^2\right)\right] = -\sigma\nabla\cdot\mathbf{E}\,, \qquad (9)$$

$$\nabla\times(1/\sigma\,\nabla\times\mathbf{H} - L\nabla p) = -\mu\,\partial\mathbf{H}/\partial t\,. \qquad (10)$$

Equation (7) and equation (10) describe the mechanical and electromagnetic wave fields, respectively. All coupling is present in the transport equations (8)-(9). The conversion between seismic and electromagnetic energy at an interface between regions with different parameters is simulated in our modelling only for the PSVTM coupling, i.e. the compressional (P wave) and vertical polarized shear waves (SV wave) generate electrical currents in the PSV particle motion plane. These currents couple to the EM-wavefield components with transverse magnetic polarization (TM mode) (Haartsen and Pride 1997). It is a mode of the electromagnetic field that involves only one component of the magnetic field and the two components of the electric field perpendicular to the considered magnetic component, e.g. the *z*-component of the magnetic field and *x*- and *y*- components of the electric field. The TM mode is useful in describing 2D models in which the magnetic field is perpendicular to the 2D plane of the model. Therefore we consider in-plane induction currents for 2D models implemented in COMSOL Multiphysics. The in-plane induction currents represent a 3D situation where there is no variation in the z direction and the electromagnetic field propagates in the *x*-*y* plane. For this case, Maxwell's equations can be reduced to a single scalar equation for the magnetic field component. This simplification can be expressed as follows:

$$\mathbf{H}\,(x,y,t) \;\xrightarrow{yields}\; H_z(x,y,t),$$

$$\mathbf{E}(x,y,t) = E_x(x,y,t) + E_y(x,y,t)\;. \qquad (11)$$

If the magnetic field is perpendicular to the modelling plane, equation (10) becomes a scalar equation with the transversal component H_z being the only field component:

$$\nabla\times(1/\sigma\,\nabla\times H_z - L\nabla p) = -\mu\,\partial H_z/\partial t\,. \qquad (12)$$

Equation (12) is well known as the induction equation for the *H* polarization (e.g. Schmucker and Weidelt, 1975) with an additional term due to the streaming potential; it is used instead of equation (10) for our modelling.

By eliminating the fluid acceleration term in equation (1) (e.g. Zienkiewicz et al. 1999) we have achieved a reduction of unknowns in the system of equations compared to conventional modelling approaches (e.g. Haartsen and Pride 1997; Haines and Pride 2006). However, along with this numerical simplification there is some loss of accuracy. This is accepted because of the benefits in terms of computation time.

2.2 The numerical setup

Here we describe the numerical implementation of the reduced set of equations derived in the section above. The modelling is done with the software package COMSOL Multiphysics. For robustness, the equations are solved using implicit time-stepping methods. The unconditional stability and ability to suppress numerical oscillations of these methods is important, as small elements may be necessary to resolve wave structures near interfaces, and time steps beyond unity grid Courant numbers (see below) are used. The limiting step size where the numerical damping becomes roughly equal to other errors, notably spatial discretization errors, is closely related to the Courant number (Courant et al. 1956), which is defined as:

$$CFL = c\Delta t/h\;, \qquad (13)$$

where c is the maximum wave speed, h is the grid spacing, and Δt is the time step size. As seismic source we used a Ricker wavelet with a 380 Hz centre frequency. The frequency was chosen on the basis of the finite-element size and resolving power of the spatial discretization.

Since our model allows examination of the entire domain at a fixed point in time, or of a single point throughout the duration of the simulation, a full analysis of the different wave modes is possible. The coseismic wave and the interface responses are the most prominent and we will investigate where these waves originate and how they propagate. It is important to avoid spurious reflections in the model which would negatively affect the accuracy of the numerical solution. Therefore non-reflecting boundary conditions are applied, which damp the wave motion near the boundaries. Non-reflecting boundary conditions allow an outgoing wave to leave the modelling domain with no or minimal reflections. For the case of transient analysis, Givoli`s and Neta`s reformulation of the Higdon conditions (Givoli and Neta, 2004) for plane waves was implemented.

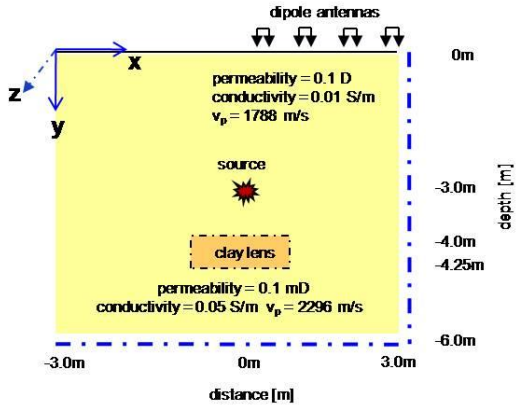

Figure 1: 2D model setup featuring a clay lens at 4 m depth in a sand background, a subsurface seismic shot point, and an electrode receiver line at the ground surface.

To simulate the seismoelectric effects in a porous medium, we used a simple model illustrated in Figure 1 that involves a clay lens in a sand background. The material properties for this setup are shown in the figure. We are particularly interested in the ability of the seismoelectric method to detect thin subsurface layers. The source/receiver configuration is also depicted in Figure 1. The explosion source is positioned nearly in the middle of the model 1 m above the clay lens. The receivers are arranged symmetrically at both sides of the source at the ground surface. The receiver spacing is 0.03 m. The example has the following medium parameters. The porosity ϕ is 30% in the sand. All layers are saturated with pore water of pH 7, salinity 0.001 mol/L, and a viscosity η of 10^{-3} Pa s. The Zeta potential is calculated using the relations provided by Pride and Morgan (1991) and therefore the corresponding electrokinetic coupling coefficient is set to L = 4.9e-7 m^2/Vs. The permeability k is 0.1 D in the sand background and 0.1 mD in the clay lens. The electrical conductivity σ is 0.01 S/m in the sand background and 0.05 S/m in the clay lens.

3. Results

3.1 The seismoelectric effects

It has been theoretically shown that when a seismic wave propagates through a fluid-saturated porous medium, seismoelectric coupling phenomena generate EM disturbances of three different types (Haines 2004). The first type is called direct field, because it can be thought of as analogous to the seismic direct wave. It is generated by charge separation at the impact point caused by the fluid pressure distribution and it occurs at the time of the source impulse and continues until the region of the impact point has relaxed to its original state (Figure 2a). The second effect occurs when a seismic wave travels through a porous material, creating a fluid pressure gradient and an acceleration of the grain matrix. The associated charge separation manifests an electric field, collocated with the seismic wave; it is called coseismic field (Figure 2b). The third effect occurs when a mechanical disturbance encounters an interface in material properties. When crossing an interface between two layers with different properties, a seismic wave generates a time-varying charge separation which acts as a dipole radiating electromagnetic energy independently of the seismic wave. Due to constructive interference, a significant portion of the first Fresnel zone acts as a disk of electric dipoles oriented normal to the interface. This disk of dipoles oscillates with the waveform of the seismic wave (Figure 2c).

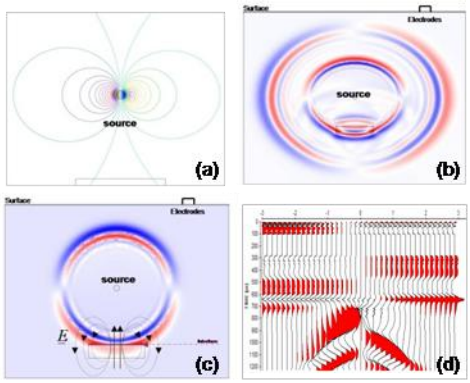

Figure 2: Snapshots of the different seismoelectric phenomena (a-c) and their corresponding seismoelectrogram (d): a) direct field. b) coseismic field. c) interface response. d) seismoelectrogram. The effects are simulated for an identical setup (Figure 1) and model parameters, but results at different times are shown.

The synthetic seismoelectrogram in Figure 2d shows the three different types of seismoelectric phenomena. The different types of signals in the seismoelectrogram are corresponding to the characteristics of the seismoelectric effects shown in the Figures 2a-c. The dipoles of the direct field and the interface response are recorded at nearly the same time at all electrodes because of the high velocities of EM waves relative to seismic waves. The coseismic field shows the typical hyperbolical structure of a seismic wave. All signals show a polarity reversal at the lateral position of the shot point.

3.2 The responses of the system

To gain insight into the coupling of the different seismoelectric responses we computed the electric, magnetic, and displacement fields generated by the same point source and plotted them in one figure (Figure 3). To describe the dynamical aspects of the system a new approach is adopted in form of the von Mises stress (Kröger 2007). The von Mises stress is composed of the absolute value of the resulting stress tensor and the mixed terms of the single components of the transversal contraction (e.g. Zienkiewicz 1999).

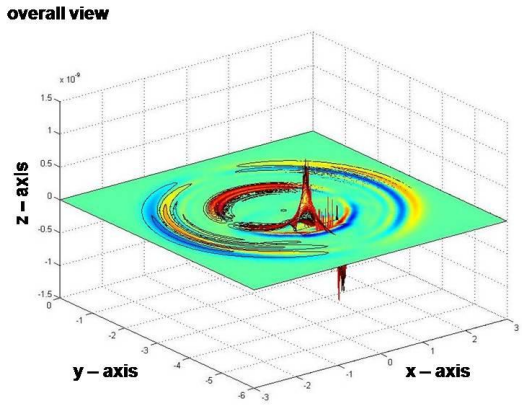

Figure 3: Electric potential (surface plot), von Mises stress (contour plot), and horizontal component of the magnetic field (height plot) at t = 1.2 ms. The TM wave develops when the SV wave encounters the interface of the clay lens.

The fields are plotted for the time when the trough of the shear wave arrives at the clay lens (t = 1.2 ms). Figure 3 shows that the horizontal displacement of the P wave and the vertical displacement of the SV wave are delineated by the von Mises stress. Furthermore, the snapshot points out that the electric and magnetic fields are locally induced by the propagation of P and SV waves through the fluid-saturated porous medium, i.e., the converted magnetic field is caused by the SV wave at the interface ("interface response") and the induced electric field is caused by the displacement components of the waves ("coseismic field").

To investigate the TM wave field conversions in more detail, snapshots and a synthetic magnetogram were calculated for the different mechanical contrasts of the model. The snapshots are plotted at the time of arrival of the maximum of the peak and trough of the SV wave at the upper boundary of the clay lens at t = 1.07 ms and t = 1.20 ms, respectively (Figure 4a), and arrival of the maximum of the peak and trough of the SV wave at the lower boundary of the clay lens at t = 1.29 ms and t = 1.39 ms, respectively (Figure 4b). The snapshots show the mechanical displacement of the SV wave (contour plot) and the resulting magnetic field component (surface plot). The latter reveals an dipole radiation pattern, centred under the seismic source on the interface and with field lines pointing on one side into the paper and on the other side out of the paper.

Figure 4a

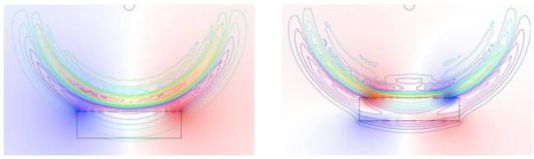

Figure 4b

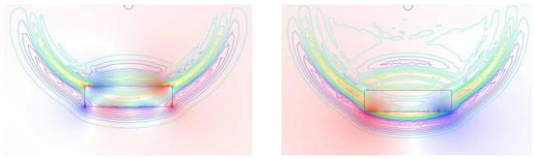

Figure 4: (a) Snapshots calculated for the time of arrival of the maximum of the peak at t = 1.0 ms (left) and the trough at t = 1.2 ms (right) of the wave at the upper boundary of the clay lens. (b) Snapshots calculated for the time of arrival of the maximum of the peak at t = 1.29 ms (left) and the trough at t = 1.39 ms (right) of the wave at the lower boundary of the clay lens. The two successive snapshots show both the mechanical displacement of the SV wave (contour plot) and the resulting magnetic dipole field (surface plot).

The magnetogram (Figure 5) is computed for the set of receivers at the ground surface for the same time interval as for the snapshots (t = 0.9-1.4 ms). It shows the conversion of the SV wave to TM waves in form of the H_z component of the magnetic field occurring at the upper and lower boundaries of the clay lens. Comparing with Figures 4a-b, one can see the good correspondence between the dipoles in the snapshots and those in the magnetogram. The maxima and minima of the amplitudes in the magnetogram coincide exactly with the peaks and troughs of the wave when encountering the interface.

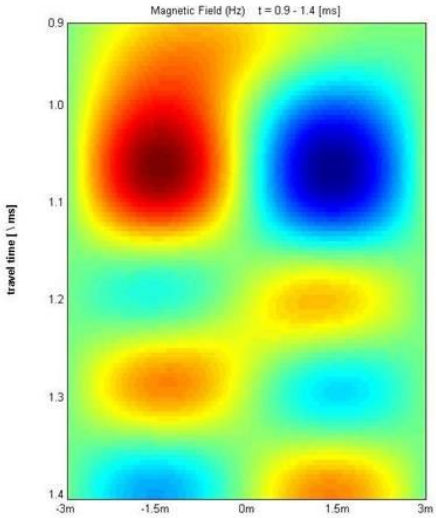

Figure 4: Seismoelectric conversion of wavefields for the PSVTM coupling. The magnetogram shows for the time interval t = 0.9-1.4 ms the gradual TM wave conversion at the upper and lower boundaries of the clay lens.

4. Conclusions

We have investigated seismoelectric effects that occur in the shallow subsurface by means of finite-element modelling using COMSOL Multiphysics. Such simulation studies are important to assess the potential use of the seismoelectric method for the characterization of the subsurface and its fluid content. Our simulations revealed the three kinds of seismoelectric effects which are predicted by the theory: direct field, coseismic field, and interface response. Our numerical code can be used to study the interaction of seismic and EM wave propagation as a function of the material properties of a fluid-saturated medium. Its main application is to simulate the EM waves generated by the passage of seismic waves through an interface separating two different media. The modelling results indicate that the seismoelectric method can detect thin, interbedded layers and lenses.

5. References

1. Biot, M., Theory of propagation of elastic waves in a fluid-saturated porous media, *J. Acoust. Soc. Am.*, **28**, 168-178 (1956a).

2. Courant, R., Friedrichs, K. O., and Lewy, H., On the partial difference equations of mathematical physics, *IBM Journal*, **11**, 215-234 (1956).
3. De Groot, S. R., *Thermodynamik irreversibler Prozesse*, Bibliographisches Institut AG, Mannheim (1960).
4. Garambois, S., and Dietrich, M., Full waveform numerical simulations of seismoelectromagnetic wave conversions in fluid-saturated stratified porous media, *J. Geophys. Res.*, **107**, ESE 5, 1-18 (2002).
5. Givoli, D., and Neta, B., High-order non-reflecting boundary scheme for time-dependent waves, *Journal of Computational Physics*, **186**, 24-46 (2003).
6. Groot, S., and Mazur, P., *Non-equilibrium Thermodynamics*, Dover Pubn Inc, New York (1984).
7. Haines, S., Seismoelectric imaging of shallow targets, *PhD thesis*, Stanford University (2004).
8. Haines, S., and Pride, S., Seismoelectric numerical modeling on a grid, *Geophysics*, **71**, N57-65 (2006).
9. Haartsen, M. W., and Pride, S., Electroseismic waves from point sources in layered media, *J. Geophys. Res.*, **102**, 24745-24769 (1997).
10. Kröger, B., Modellierung und Sensitivitäts-analysen für Seismoelektrik mit Finiten Elementen, *Diploma thesis*, Technical University Berlin (2007).
11. Pride, S., Governing equations for the coupled electromagnetics and acoustics of porous media, *Physical Review B*, **50**, 15678-15696 (1994).
12. Pride, S., and Haartsen, M. W., Electroseismic wave properties, *J. Acoust. Soc. Am.*, **100**, 1301-1315 (1996).
13. Pride, S., and Morgan, F. D., Electrokinetic dissipation induced by seismic waves, *Geophysics*, **56**, 914-925 (1991).
14. Schmucker, U., and Weidelt, P., *Electromagnetic induction in the earth: Lecture Notes*, Aarhus (1975).
15. Wang, H. F., *Theory of linear poroelasticity*, John Wiley & Sons, New York (2000).
16. Wurmstich, B., and Morgan, F. D., Modeling of streaming potential responses caused by oil well pumping, *Geophysics*, **59**, 46-56 (1994).
17. Zienkiewicz, O. C., Chan, A. H. C., Pastor, M., Schrefler, B. A., and Shiomi, T., *Computational geomechanics*, John Wiley & Sons, New York (1999).